Title

Uncertainty quantification of damage detection features derived from frequency response models

ISBN

978-1-138-00120-6

Authors

Mao, Z
Todd, MD

Publication Date

2015

DOI

10.1201/b17618-158

Peer reviewed

Uncertainty quantification of damage detection features derived from frequency response models

Z. Mao & M. D. Todd*
Department of Structural Engineering, University of California San Diego, La Jolla, CA 92093-0085, USA
**Corresponding author; email: mdtodd@ucsd.edu*

ABSTRACT: System identification in the frequency domain plays a fundamental role in many aspects of structural health monitoring (SHM). Frequency domain approaches all typically involve estimation of a transfer function, the most common of which is the usual frequency response function (FRF). The FRF serves as a fundamental basis from which many features are derived that are used for detection, localization, and even quantification of damage in structures. Fundamentally, SHM must involve hypothesis testing, since inevitably estimated FRFs involve uncertainty or noise at all stages of the measurement and estimation process. Regardless of source, these errors propagate to the final decision-making process, resulting in either classification rate performance reduction or false positive detection increases. This paper builds an uncertainty model for FRF magnitude and phase estimation and uses receiver operating characteristic curves to evaluate the model's performance on data from a plate-like structure.

1 INTRODUCTION

System identification in the frequency domain plays a fundamental role in many aspects of structural engineering. Various applications of system identification widely span from system design, model/test correlation and updating, verification and validation activities, structural control, and structural health monitoring (Ljung, 1982). Frequency domain approaches, generally considered superior for estimation and computational purposes (Brincker, 2001), typically involve estimation of transfer functions, whether it is the usual frequency response function (FRF) or an output-to-output transfer model such as transmissibility. The field of structural health monitoring (SHM), which detects assesses structural health via features mined from in-situ measured structural performance data, has proposed large classes of features derived from estimations of either conventional FRF or transmissibility.

Any frequency domain approach requires knowledge of the input excitations (in the case of FRF) and output responses (in all cases). For all practical applications, regardless of frequency domain model chosen or its intended use, uncertainties affect the process. It is well known that the sensitivity of any feature derived from FRF is compromised by noise, generally categorized into four classes: operational, environmental, measurement, and computational (Johnson, 2002); these compromised estimates may lead to significant false-positive (Type-I) errors in the interpretation of system identification results (Kay, 1998).

In the common binary case of structural damage assessment and detection, two different conditions are compared, namely undamaged baseline and damaged testing conditions. Inevitably, the decision associated with correct classification of the features being used is corrupted by the uncertainty or noise induced by the processes above. Regardless of source, this noise leads to the propagation of uncertainty from inception to final estimation of the feature, and makes the final evaluation of features a random variable process. Distinguishing the two conditions is thereby evaluated by some form of a classical binary hypothesis test.

In this paper, a statistical model for uncertainty in the FRF estimation process is established, and a probability density function is derived which is exploited in the hypothesis test. The established uncertainty quantification models are validated with outlier analysis for the conditions with good signal quality and poor quality with extraneous noise contamination. Based upon the statistical model, ultimate hypothesis testing is deployed to characterize the performance of FRF-based damage detection, and optimal rate of detection given certainty tolerance of false alarms is obtained. Finally, receiver operating characteristics (ROC) and the area under the ROC curve are used to evaluate the performance

of detection and suggest optimal trade-off between detection rate and false alarm rate.

2 FRF UNCERTAINTY QUANTIFICATION

2.1 FRF Estimation

Considering a single-input-multiple-output (SIMO) signal flow shown in Figure 1, *u* and *v* denote true input and output of arbitrary vibration measurements, and *i* and *j* represent two sensing locations and channels. With additive noise *m* and *n*, the actual measurements obtained from data acquisition hardware are denoted as *x* and *y*, as in Figure 1.

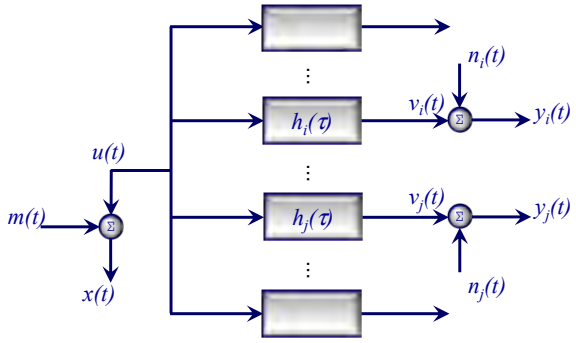

Figure 1. SIMO data flow.

Mathematically, the FRF is defined as the ratio between frequency domain input and output

$$H_i(\omega)=\frac{V_i(\omega)}{U(\omega)}, \tag{1}$$

in which $U(\omega)$ and $V(\omega)$ are the Fourier transforms of ideal ("noise free") input and output. Given the fact that signal *u* and *v* are not actually measureable because they are always contaminated by noise, different algorithms (called estimators) are often adopted to calculate the estimations, such as

$$\hat{H}_i(\omega)=\frac{\hat{G}_{xy_i}(\omega)}{\hat{G}_{xx}(\omega)}. \tag{2}$$

In this estimator, FRF is calculated via auto and cross power density function estimations given by Welch's method

$$\hat{G}_{xy}(\omega)=\frac{1}{n_d}\sum_{k=1}^{n_d}\tilde{X}_k^*(\omega)\cdot\tilde{Y}_k(\omega), \tag{3}$$

where n_d is number of averages, * denotes complex conjugate, and $X(\omega)$ and $Y(\omega)$ are the Fourier transforms of $x(t)$ and $y(t)$ (Welch, 1967).

2.2 Uncertainty Quantification

Uncertainty quantification (UQ) in this paper aims to model the estimation process as a random variable in order to obtain a probability density function, from which any statistical information regarding the estimation can be achieved. For a Gaussian process of a vibration-based structural test, normality of the excitation will be propagated to the output if the mechanical channel is linear, along with any sort of variability and noise contaminating the measurements. Therefore it is reasonable to statistically model the uncertainty of FRF via a Gaussian-related approach, particularly since frequency domain averaging, as shown in Equation (3), strengthens it by the central limit theorem.

By making Gaussian assumptions at the level of fundamental variability in the cross- and autopower spectra of Equation (2), the distributions of FRF magnitude and phase estimations are characterized by the probability density function in Equations (4) and (5) (Mao, 2013) for the magnitude:

$$p_{|\hat{H}|}(H)=\frac{\gamma}{\pi\alpha}\cdot e^{-\frac{1}{2(1-\rho^2)}\left(\frac{\mu_A^2}{\sigma_A^2}-2H\frac{\mu_A\mu_C}{\sigma_A\sigma_C}+\frac{\mu_C^2}{\sigma_C^2}\right)} + \frac{\beta}{\sqrt{2\pi}\alpha^{3/2}}\cdot e^{-\frac{(H\mu_A-\mu_C)^2}{2\alpha}}\cdot\mathrm{Erf}\left(\frac{\beta}{\sqrt{2\alpha}\gamma}\right), \tag{4}$$

in which g_A and g_C are the sampled magnitudes of auto- and cross-power spectra, and

$$\alpha=H^2\sigma_A^2-2\rho H\sigma_A\sigma_C+\sigma_C^2,$$
$$\beta=H\sigma_A\left(\rho\mu_A\sigma_C-\mu_C\sigma_A\right)+\sigma_C\left(\rho\mu_C\sigma_A-\mu_A\sigma_C\right)$$
$$\gamma=\sqrt{1-\rho^2}\sigma_A\sigma_C \quad ;$$
$$\rho=\frac{\mathrm{cov}\left(g_A,g_C\right)}{\sigma_A\sigma_C}$$

and for the phase,

$$p_{\angle\hat{H}}(\theta)=\frac{e^{-\frac{\mu_R^2+\mu_I^2}{2\sigma^2}}}{2\pi} + \frac{\eta\cdot e^{-\frac{\left(\mu_R\sin(\theta)-\mu_I\cos(\theta)\right)^2}{2\sigma^2}}}{2\sqrt{2\pi}\sigma}\left(1+\mathrm{Erf}\left(\frac{\eta}{\sqrt{2}\sigma}\right)\right), \tag{5}$$

where

$$\eta=\mu_R\cos(\theta)+\mu_I\sin(\theta).$$

All the σ and μ terms represent the standard deviations and mean values of the corresponding time series.

3 STATISTICAL MODEL VALIDATION

3.1 Test design

In order to validate the proposed UQ model, a lab-scale test structure is built as shown in Figure 2. Random excitation is applied onto the cantilever plate and acceleration responses at multiple locations are measured. Equations (4) and (5) give the uncertainty bounds corresponding to a given significance level, therefore outliers observed in Monte Carlo test are adopted as the metric to validate the probability density functions. The UQ models are validated if the outlier percentage is consistent with the complement of confidence level.

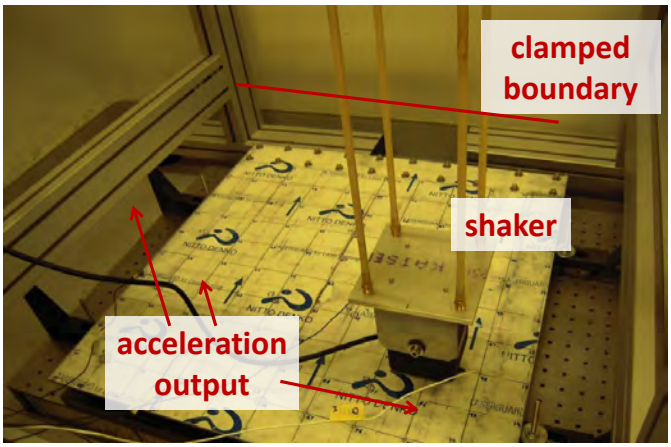

Figure 2. Test structure for model validation.

The test is implemented in a lab environment where noise influence is relatively low, but the data acquired are still considered as contaminated data $x(t)$ and $y(t)$ in Figure 1. To simulate a more realistic in-situ testing environment, the data obtained from plate structure are contaminated with extra artificial white noise to make the estimates more realistic. The original data were modified with 20 dB signal-to-noise (SNR) contamination case, which is equal to a 10% noise level in terms of energy.

3.2 UQ results

For the test and estimations with original and contaminated data, Figure 3 plots the FRF magnitude and phase between the input and an arbitrarily selected output, with uncertainty bounds associated with 90% confidence levels. The expectation is also calculated by integrating order statistics from the established probability density function. With the same number of averages (n_d), the extraneous noise causes much more fluctuation and uncertainty in both the magnitude and phase estimations, as would be expected.

As a function of frequency, FRF is evaluated at every frequency point, and at a sample frequency line, numerous realizations (trials) form a histogram, which can be compared with the established probability density models, as shown in Figure 4. There is very good consistency, indicating the probability density function characterizes FRF magnitude and phase distributions accurately, and green stars are the 5% and 95% significance levels at a given 90% confidence.

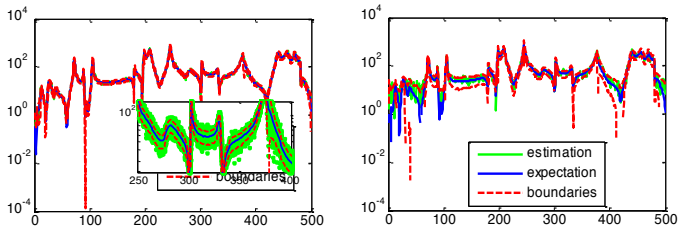

(a) magnitude estimation; noise free

(b) magnitude estimation; noise contaminated

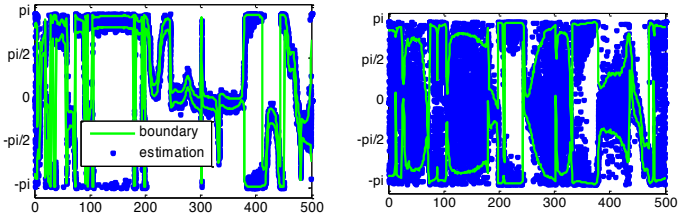

(c) phase estimation; noise free

(d) phase estimation; noise contaminated

Figure 3. FRF estimations and 90% confidence uncertainty boundaries.

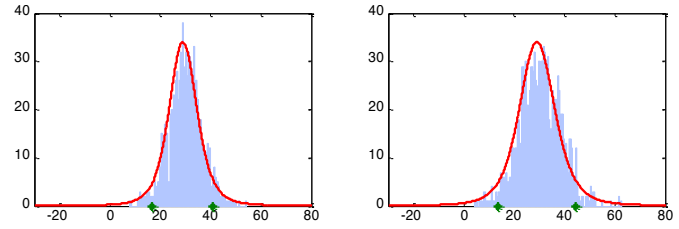

(a) magnitude estimation, noise-free

(b) magnitude estimation, noise-contaminated

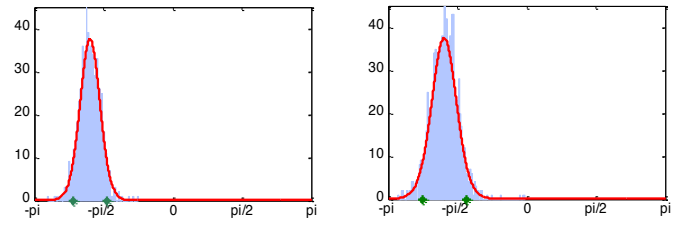

(c) phase estimation, noise-free

(d) phase estimation, noise-contaminated

Figure 4. Histogram of FRF estimations at single frequency line with characterized distribution and 90% quantiles.

A quantified consistency validation is implemented with outlier percentage used as the quality metric. Different confidence thresholds are selected,

namely 95%, 90%, 80% and 70%, and outlier percentage are plotted across the entire frequency domain. Figures 5-8 plot the results in crossings, with the anticipated value, i.e., 1%, 5%, 10% and 25%, plotted with a red line. Multiple thresholds are adopted here for a thorough model validation. Figures 5 and 6 illustrate the validation result of magnitude UQ model, with original data and the data contaminated with artificial noise. For the extraneous noise-free condition, the observed outliers are consistent with threshold confidence, and the UQ model works well across all frequency lines.

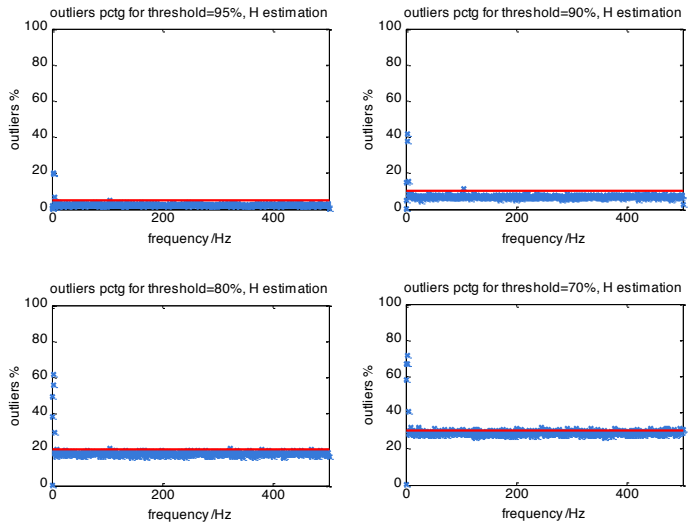

Figure 5. Outlier percentage in FRF magnitude observations, extraneous noise free condition.

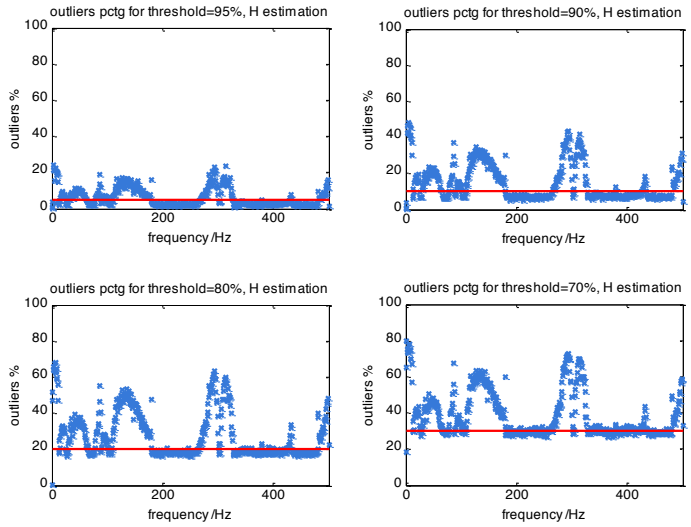

Figure 6. Outlier percentage in FRF magnitude observations, noise contaminated condition.

For the stricter condition with extraneous noise, as Figure 6 shows, the model performance is degraded and at some frequencies, the consistency of outlier percentages is poor. This phenomenon is caused by the limitation of Gaussian assumption in the UQ process. With noisy data and few averages, the Gaussian assumption cannot fully describe the actual distribution, and leads to a violation of domain support.

Similar to magnitude uncertainty, Figures 7 and 8 illustrate the validation result of phase estimation uncertainty. The UQ model works perfectly for the original data obtained in the lab, and also nicely for the contaminated condition, with a slight degradation. Compared to the magnitude validation, the results in phase uncertainty quantification are obviously more robust to extraneous noise. From Figures 5 to 8, the UQ models are validated with outlier analysis, and when there is extraneous noise, the performance of UQ is degraded, especially for magnitude estimations.

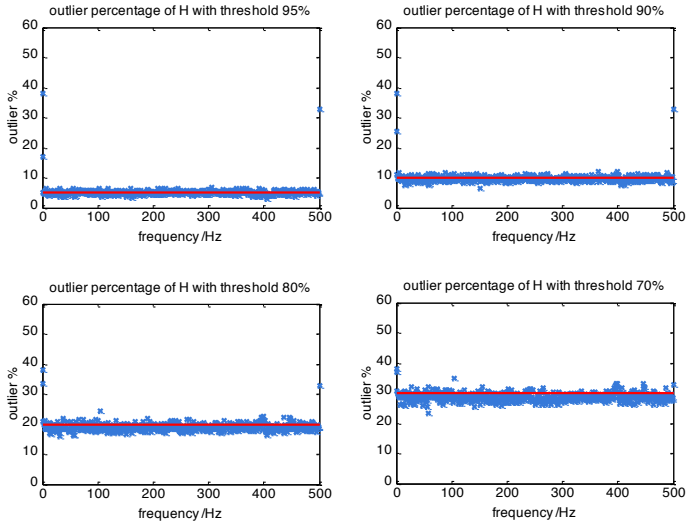

Figure 7. Outlier percentage in FRF phase observations, extraneous noise free condition.

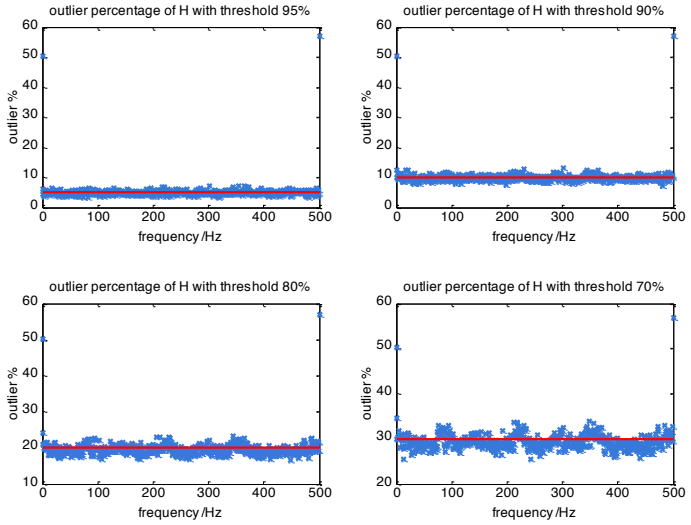

Figure 8. Outlier percentage in FRF phase observations, noise contaminated condition.

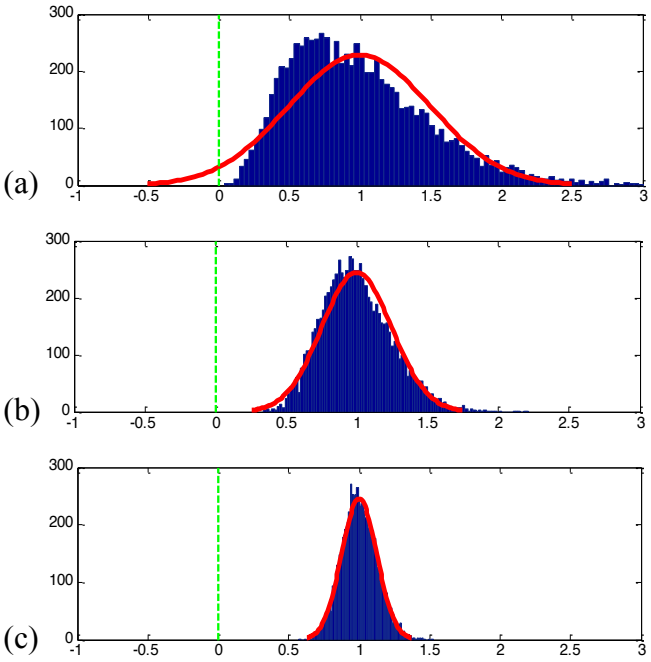

Figure 9. Normality with different amount of averaging, (a) n_d=8; (b) n_d =32; (c) n_d =128.

This is mainly caused by the violation of distribution support, and Figure 9 addresses this issue by a parametric study. As shown in Figure 9, when the mean value of the random variable is small, with sufficient variance, the skewness will cause the left tail of distribution to penetrate into negative side. Under this circumstance, it is inappropriate to apply the Gaussian assumption, which has a full real number domain support. By taking more averages, the variation of distribution is suppressed, and the left tail does not substantially cross zero. As a result, the performance of UQ model present is improved with more averaging if the SNR is poor. In this test, the lab-acquired data acquired is only enough for 20 averages, thus the negative tails appear in the contaminated condition.

4 HYPOTHESIS TESTING

4.1 Damage test-bed

In order to make changes to the structure, an external spring is placed underneath the plate at an arbitrary place as surrogate damage, as shown in Figure 10. The general idea is to detect change of FRF magnitude/phase from uncertain test data. With a supervised learning process, baseline statistics and damaged statistics are both available, and the damage detection process is to determine the statistical significance of FRF feature evaluation. In the process, a null hypothesis is made that there is no statistical significance to the case of the system being damaged, and the alternative hypothesis that damage to the system has occurred with statistical significance.

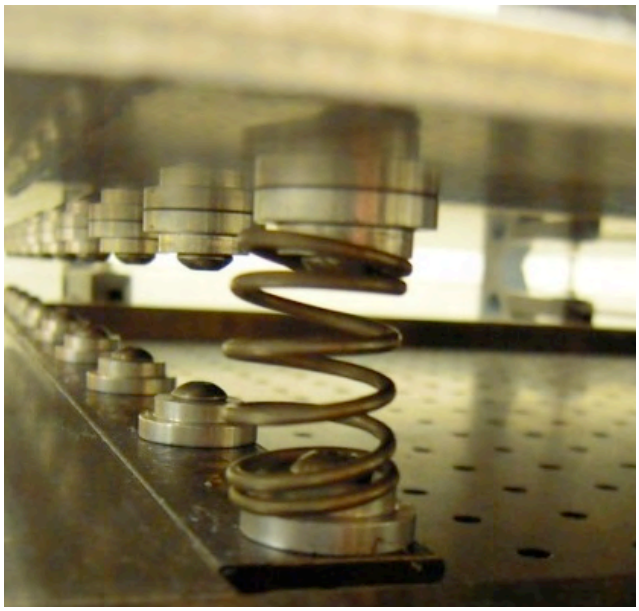

Figure 10. Surrogate damage simulation by added spring.

Equation (6) describes the null and alternate hypotheses, which partition the decision-making process into acceptance or rejection of given statistical hypotheses under certain confidence:

$$\begin{aligned} \mathcal{H}_0 &: z:\ \Phi(\mathbf{\Lambda}_u) \\ \mathcal{H}_1 &: z:\ \Phi(\mathbf{\Lambda}_d) \end{aligned} \tag{6}$$

which means a classification between undamaged and damaged distributions, so the separation of two distributions $\Phi(\Lambda_u)$ and $\Phi(\Lambda_d)$ is essential to the quality of hypothesis test.

4.2 Detection rate and errors

Given any detection threshold γ, the hypotheses in Equation (6) can be rewritten as Equation (7):

$$\begin{aligned} \mathcal{H}_0 &: z \le \gamma \\ \mathcal{H}_1 &: z > \gamma \end{aligned} \tag{7}$$

assuming that damage will cause an increase in the FRF features. As shown in Figure 11, the corresponding rates of detections and false alarms are calculated as the area under probability density curves.

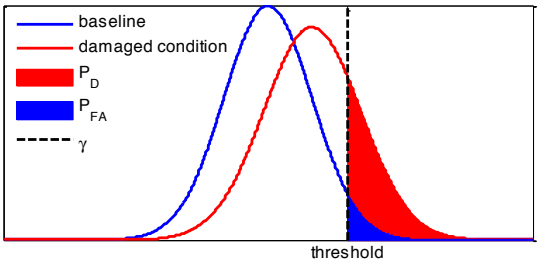

Figure 11. True positive and false positive for hypothesis test.

There are two types of errors, namely false positive (type I) and false negative (Type II). Type I error is a false alarm when a true null hypothesis is rejected, and type II error is the cases that false null hypothesis fails to be rejected (Kay, 1998). As the decision threshold is varied between the two data cases, the true positive rate and false positive rate under transformed null/alternative hypotheses will change monotonically with each other. As an example, Figure 12 plots the undamaged and damaged FRF magnitude distributions subject to different level of noise contamination. Probability of detection and probability of false alarms can be calculated by integrating the appropriate probability density curves.

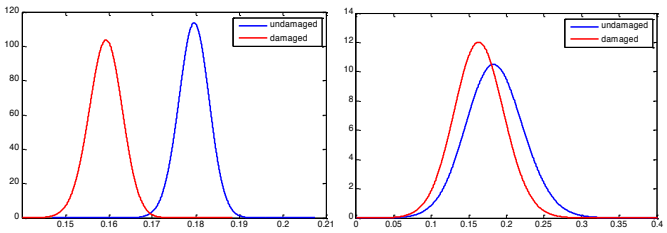

Figure 12. Baseline and damaged distributions for plate about original data and contaminated data

Since the probability of detection increases as the rate of false alarms, Figures 13 and 14 plot the maximum possible rate of detection given a fixed false alarm tolerance. Moreover, we can execute the hypothesis test at all frequency lines, therefore the two figures plot detection rate P_D given P_{FA} equal to 10%, 1%, and 0.1%, as a function of frequency. Figures 13 and 14 illustrate the results from original data and contaminated data, respectively, and it is clear that when the tolerance of false positive is small, the rate of detection moves down in a quasi-parallel fashion, for both noise contamination circumstances. With no doubt, the noise contamination dramatically degrades the rate of detection, and only leaves a very limited frequency region with high quality of detection.

Comparing magnitude to phase detection, Figure 15 illustrates the detection rate given a 10% tolerance of false positives, and the data is contaminated by extraneous noise. There are only several frequency lines with very good detectability, and they are consistent between the magnitude and phase testing.

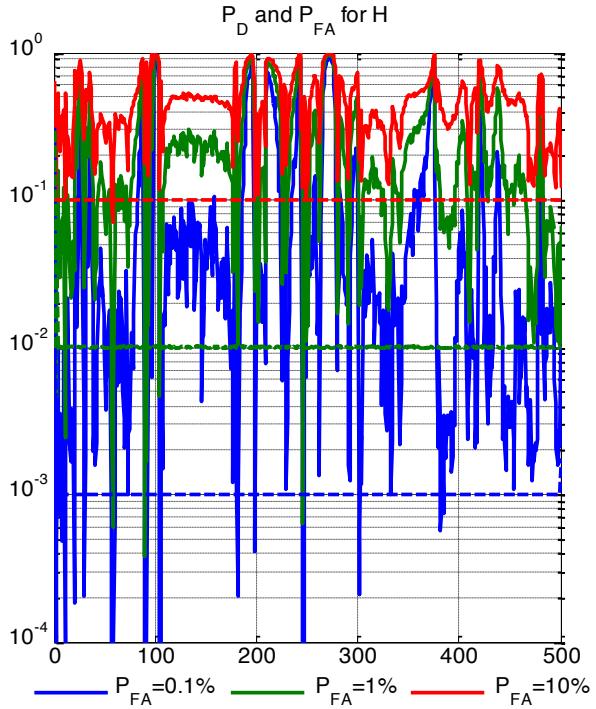

Figure 13. Detection rate versus different levels of false alarms using FRF magnitude; extraneous noise-free.

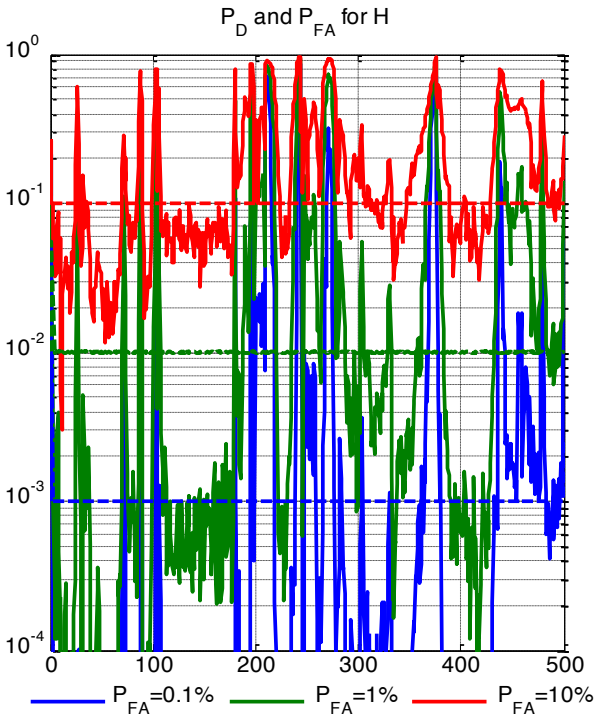

Figure 14. Detection rate versus different levels of false alarms using FRF magnitude; extraneous noise-contaminated.

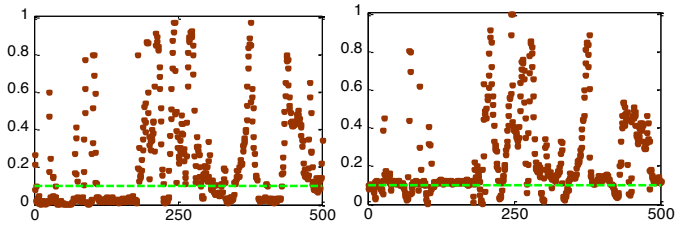

Figure 15. Detection rate given 10% of P_{FA}, extraneous noise-contaminated, (left: magnitude; right: phase).

4.3 Receiver operating characteristics (ROC)

As mentioned above, the rate of detection is monotonically correlated with the false positive rate, and a receiver operating characteristic (ROC) curve may be used to quantify this. A ROC curve is traced out parametrically as the decision boundary between choosing the hull and alterative hypotheses is varied. As Figure 16 illustrates, if it goes to the upper left corner, it means the optimized detection will have a nearly 100% detection rate, practically independent of false alarms. On the other hand, the 45-degree diagonal line is the random guess performance, which means equal detection and false alarms (effectively akin to coin flipping). Figure 16 shows the performance of the model at a single frequency line. At this sample frequency line, the noise free condition shows significantly enhanced detectability (blue line). As noise is added, one may quantitatively observe the performance degradation (red curve), which for severely compromised signal-to-noise, would approach the green curve ("coin flip").

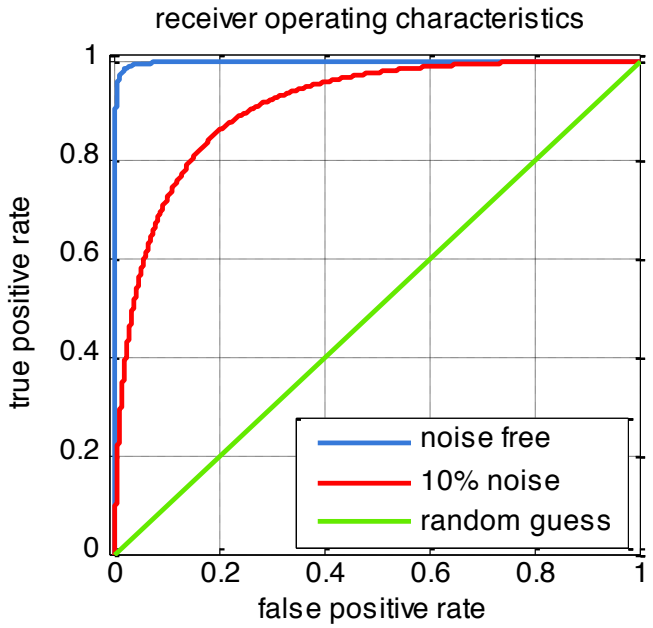

Figure 16. ROC curves at a sampled frequency line.

One way to reduce comparisons with noise to a single metric is to introduce the area under the ROC curve (AUC) metric, which is the total area between one ROC curve and the 45-degree random guess line, as demonstrated in Figure 17. This metric varies from 0 to 0.5, and there are a couple of further normalizations adopted in the literature. In this paper, the area is normalized by its maximum value (0.5), and therefore the best ROC with perfect detection performance will have AUC equal to 1.

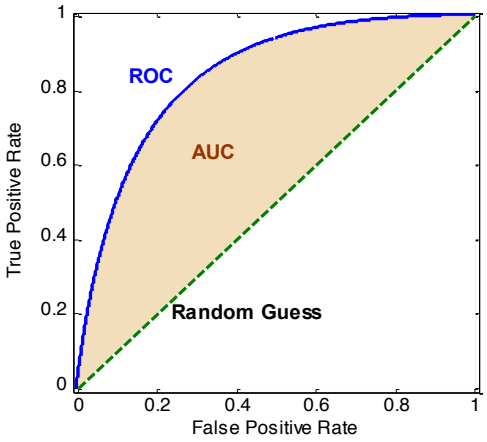

Figure 17. Area Under Curve (AUC) definition.

The result in Figure 18 plots AUC of magnitude detection across entire frequency domain for the contaminated case, and unsurprisingly, all the AUC metric degrades as noise contamination goes severe. The shape of this curve is close to the probability of detection in Figures 13 and 14, and this illustrates the consistency, i.e. better performance of detection (in terms of AUC) will lead to a higher detection rate (P_D) given certain false positive tolerance (P_{FA}).

In Figure 18, even under the 10% noise-to-signal contamination, there are several frequencies at which the detectability is very good, indicating that these frequency lines have high input-output gain (such as resonances) and are much more robust to noise.

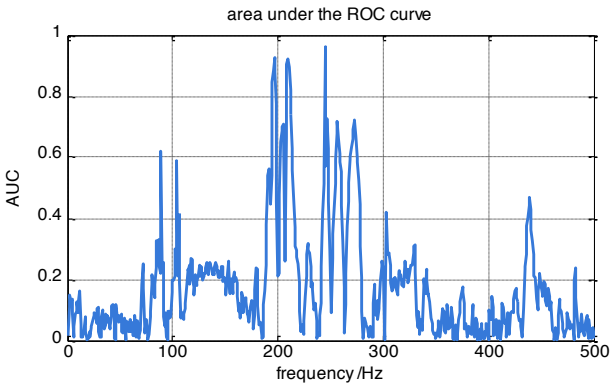

Figure 18. AUC across all frequencies.

5 SUMMARY

This paper proposes uncertainty quantification models for frequency response function magnitude and phase estimations, and probability density functions are presented to fully characterize the distribution of the estimations as random variables. The proposed models are validated by outlier analysis from Monte-Carlo test, and outlier percentage is used as metric for comparison. To be more stringent, test data obtained from a lab-scale structure are contaminated by artificial noise, which degrades the UQ performance, especially for magnitude estimations. However, it is proven that with sufficient number of averaging, the probability density function also nicely characterizes the uncertainty of estimations with Gaussian assumptions.

Hypothesis testing is deployed adopting the proposed statistical model, and optimal detection rates may be computed for any detection threshold. Changing the detection threshold will cause detection rate and false alarm rate change in a correlated way, and this may be studied via ROC curves, which leads to optimization formulations centered upon detection rates and/or false positive rejections. To generally evaluate the detectability for FRF features at an arbitrary frequency line, the metric of area under curve is adopted to evaluate the performance of significance detection quality over the frequency domain, and frequency lines with higher input-output gain, especially close to resonances, will have better detectability, even when there is extraneous noise contamination.

ACKNOWLEDGEMENT

The authors acknowledge the Air Force Office of Scientific Research for support of this work (grant FA9550-10-1-0455; Dr. David Stargel, Program Manager).

REFERENCES

Brincker, R., Zhang, P. and Anderson, P. 2001. Modal Identification of Output-Only Systems Using Frequency Domain Decomposition. *Smart Mat. Struc.* 10: 441-445.

Devriendt, G., Steenackers, G., De Sitter, G., and Guillaume, P. 2010. From Operating Deflection Shapes Towards Mode Shapes Using Transmissibility Measurements. *Mech. Sys. Sig. Proc.* 24: 665-677.

Fieller, E.C. 1932. The Distribution of the Index in a Normal Bivariate Population. *Biometrika.* 24: 3-4.

Johnson, T.J and Adams, D.E. 2002. Transmissibility as an Indicator of Structural Damage. *ASME J. Vib. Acous.* 124: 634-641.

Kay, S.M. 1998. Fundamentals of Statistical Signal Processing, Vol II - Detection Theory. Prentice Hall

Ljung, L. 1982. Aspects on the System Identification Problem. *Sig. Process.* 4: 445-456.

Mao Z. and Todd, M. D. 2013. Statistical modeling of frequency response function estimation for uncertainty quantification, *Mechanical Systems and Signal Processing*, 38: 333-345.

Welch, P.D. 1967. The use of Fast Fourier Transform for the estimation of power spectra: a method based on time averaging over short, modified periodograms. *IEEE Trans. Audio Electroacoustics.* 15: 70-73.

Worden, K., Manson, G., and Fieller, N.R.J. 2000. Damage Detection Using Outlier Analysis. *J. Sound Vib.* 229: 647-667.